International Journal of Advanced Science and Technology
Vol.92 (2016), pp.49-58
http://dx.doi.org/10.14257/ijast.2016.92.06

Numerical Investigation of the Fluid Flow around and Past a Circular Cylinder by Ansys Simulation

Mojtaba Daneshi

Department of Mechanical Engineering, Science and Research Branch, I. A. University, Tehran, Iran
M.daneshi@srbiau.ac.ir

Abstract

Flow around a circular cylinder is a fundamental fluid mechanics problem of practical importance. The dynamic characteristics of the pressure and velocity fields of unsteady incompressible laminar and turbulent wakes behind a circular cylinder are investigated numerically and analyzed simulation. The governing equations, written in the velocity pressure formulation are solved using 2-D finite volume method. In the present work is based on the cylinder diameter 10^2 Reynolds number for flow analysis slow and also turbulent based on the diameter of the cylindrical Reynolds number 10^5 as well as for the analysis of the flow around a cylindrical has been considered. The aim of this research is to investigate the influence of Reynolds number on flow parameters and verify the correctness of the calculations carried out by the governing equations of fluid mechanics-flow. Research on the hydraulic parameters of the flow around a cylinder help of ANSYS software. The frequencies of the drag and lift oscillations obtained theoretically agree well with the experimental results. The pressure and drag coefficients for different Reynolds numbers were also computed and compared with experimental and other numerical results. Due to faster convergence, 2-D finite volume method is found very much prospective for turbulent flow as well as laminar flow.

Keywords: *Numerical, Circular Cylinders, Drag Coefficient, Fluid Flow, ANSYS*

1. Introduction

A common external flow configuration involves the circular cylinder or tube in crossflow, where the flow is normal to the axis of the cylinder. If an inviscid fluid is considered, the velocity distribution over the cylinder is given by: [1]

$$u_r = u_\infty (1 - \frac{r_0^2}{r^2}) \cos\theta \tag{1a}$$

$$u_\theta = u_\infty (1 - \frac{r_0^2}{r^2}) \sin\theta \tag{1b}$$

where U_∞ is the velocity far upstream the cylinder, r_o the cylinder radius, r the radial coordinate and θ the angle measured from the forward stagnation point. At the tube surface one finds: [1]

$$u_\theta = 2u_\infty \sin\theta \tag{2}$$

and thus for $\theta = \pi/2$ the velocity on the tube surface is twice the freestream velocity. By applying the Bernoulli Equation for an inviscid fluid, the pressure coefficient C_p is found to be:

$$C_p = \frac{2(p - p_\infty)}{\alpha U_\infty^2} = 1 - 4\sin^2\theta \tag{3}$$

ISSN: 2005-4238 IJAST

For an inviscid fluid, the pressure coefficient is distributed symmetrically and an integration of the pressure distribution results in zero drag and lift forces. This is an example of the d'Alembert paradox for inviscid flow past immersed bodied. In Figure 1, the inviscid flow past a tube is shown [1].

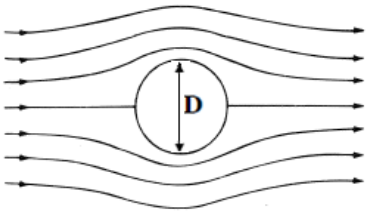

Figure 1. Schematic of a Circular Cylinder

2. Real Flow Phenomena

For viscous fluids the flow pattern is much more complicated and the balance between inertia forces and viscous forces is important. The relative importance is expressed by the Reynolds number Re_D defined as

$$Re_D = \frac{U_\infty D}{V} \tag{4}$$

where D is the tube diameter and ν the kinematic viscosity of the fluid. [1]

As the fluid approaches the front side of the tube, the fluid pressure rises from the freestream value to the stagnation point value. The high pressure forces the fluid to move along the tube surface and boundary layers develop on both sides. The pressure force is counteracted by viscous forces and the fluid cannot follow the tube surface to the rear side but separates from both sides of the tube and form two shear layers. The innermost part of the shear layers are in contact with the tube surface and moves slower than the outermost part. As a result, the shear layers roll up. The flow pattern is dependent on the Reynolds number and in Figure 2 a principal description of the various occurring flow phenomena is provided [1].

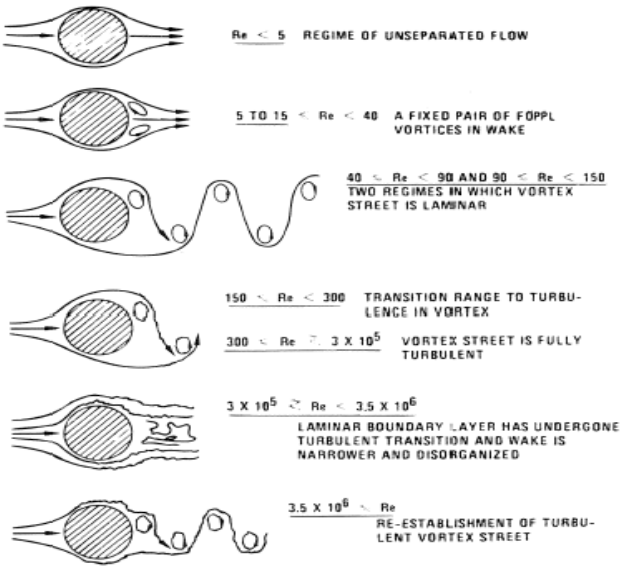

Figure 2. Regimes of Fluid Flow Across a Smooth Tube [1]

At Reynolds numbers below 1, no separation occurs. The shape of the streamlines is different from those in an inviscid fluid. The viscous forces cause the streamlines to move further apart on the downstream side than on the upstream side of the tube. In the Reynolds number range of $5 \leq Re_D \leq 45$, the flow separates from the rear side of the tube and a symmetric pair of vortices is formed in the near wake. The streamwise length of the vortices increases linearly with Reynolds number as shown in Figure 3 [2].

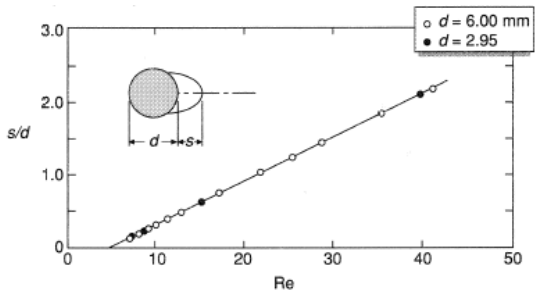

Figure 3. Streamwise Length of Vortices [2]

As the Reynolds number is further increased the wake becomes unstable and Vortex Shedding is initiated. At first, one of the two vortices breaks away and then the second is shed because of the nonsymmetric pressure in the wake. The intermittently shed vortices form a laminar periodic wake of staggered vortices of opposite sign. This phenomenon is often called the Karman vortex street. von Karman showed analytically and confirmed experimentally that the pattern of vortices in a vortex street follows a mathematical relationship, namely, [2]

$$\frac{h}{1} = \frac{1}{\pi}\sinh^{-1}\{1\} = 0.281 \tag{5}$$

where h and l are explained in Figure 4.

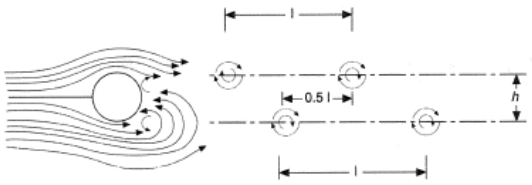

Figure 4. Model of a Vortex Street [2]

In the Reynolds number range $150 < Re_D < 300$, periodic irregular disturbances are found in the wake. The flow is transitional and gradually becomes turbulent as the Reynolds number is increased. The Reynolds number range $300 < Re_D < 1.5\times10^5$ is called subcritical (the upper limit is sometimes given as 2×10^5). The laminar boundary layer separates at about 80 degrees downstream of the front stagnation point and the vortex shedding is strong and periodic. With a further increase of Re_D, the flow enters the critical regime. The laminar boundary layer separates on the front side of the tube, forms a separation bubble and later reattaches on the tube surface. Reattachment is followed by a turbulent boundary layer and the separation point is moved to the rear side, to about 140 degrees downstream the front stagnation point. As an effect the drag coefficient is decreased sharply. For $Re_D \geq 6\times10^5$, the laminar to turbulent transition occurs in a nonseparated boundary layer, and the transition point is shifted upstream. The Re_D-range $2\times10^5 < Re_D < 3.5\times10^6$ is

in some references named the transitional range. Three-dimensional effects disrupt the regular shedding process and the spectrum of shedding frequencies is broadened. In the supercritical ReD-range, $Re_D > 3.5\times10^6$, a regular vortex shedding is re-established with a turbulent boundary layer on the tube surface [2].

3. Conceptual Overview of Flow Past a Circular Cylinder

Flow past a circular cylinder tends to follow the shape of the body provided that the velocity of the flow is very slow, this is known as laminar flow. Flow at the inner part of the boundary layers travels more slowly than the flow near to the free stream. As the speed of the flow increases, separation of flow occurs at some point along the circular cylinder due to the occurrence of the adverse pressure gradient region. Flow separation tends to roll up the flow into swirling eddies, resulting in alternate shedding of vortices in the wake region of the body known as the von Karman vortex street [3].

3.1. Pressure Distribution

The various flow phenomena are reflected in the pressure distribution on the tube surface. Figure 5 provides a few distributions of the pressure coefficient Cp and the changes in the distributions are explained by the flow mechanisms described previously [4].

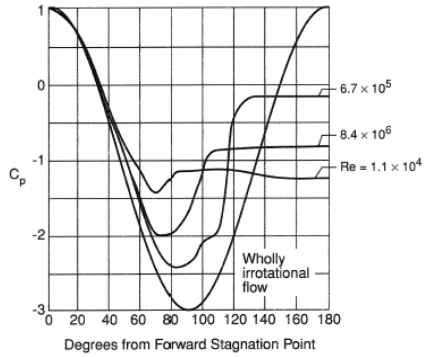

Figure 5. Pressure Distribution around the Circumference of a Tube or Circular Cylinder [4]

Particularly for $Re_D = 6.7\times10^5$, the separation of the laminar boundary layer and the reattachment is believed to be reflected in the behavior between $\theta \approx 100-110$ degrees downstream the front stagnation point. The nonsymmetrical pressure distribution result in a net force on the tube, and the existence of this force is the main cause of the pressure drop across the tube. [4]

4. Mathematical Modeling of Drag Coefficient

The total drag is generated by the friction forces and pressure forces acting on the tube. At very low Reynolds number, the drag is mainly due to friction. With an increase of Re_D the contribution of the inertia forces begin to grow so that at high Reynolds numbers the skin friction constitutes just a few per cent of the total drag. A dimensionless expression of the total drag is the drag coefficient defined by: [5]

$$C_D = \frac{\Sigma C_e}{\frac{1}{2}\rho U_\infty^2 D L} \quad (6)$$

where L is the length of the tube.

Figure 6 shows the drag coefficient as a function of Re_D.

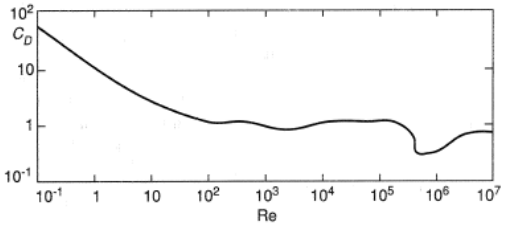

Figure 6. Drag Coefficient on a Circular Cylinder [5]

In the low Reynolds number range, C_D decreases significantly with increasing Reynolds number, mostly due to the skin friction contribution. In the subcriticai regime, the drag coefficient changes insignificantly with Re_D. As the critical flow regime is reached, the drag coefficient decreases sharply with increasing Re_D. The wake becomes narrower by the turbulent boundary layer and the associated delayed separation. At higher Re_D, C_D is increasing again probably due to the development of a turbulent boundary layer already close to the front stagnation point [6].

4.1. Factors Affecting the Flow

The crossflow past the single tube is affected by freestream turbulence, surface roughness, compressibility of the fluid and some other factors. So, for instance, the position of the transition from laminar to turbulent flow in the boundary layer depends on the turbulence level. An increase in the freestream turbulence level leads to an earlier (lower Re_D) onset of the critical flow regime and corresponding changes in the drag coefficient. Surface roughness causes an earlier onset of the critical regime and a higher drag coefficient [7].

The reported studies were concerned with circular cylinders or elliptic cylinders the flow pattern for was studied numerically by [8]-[13] for both laminar and turbulent regimes. There has not been extensive research on forces and flow around cylinder in turbulent flow. In the present article, the Fluid flows around and Past cylinder is numerically simulated.

5. Numerical Solution

This problem considers a 2D section of a circular cylinder. For the simulations presented here, depending on the geometry used, fine meshes of 50000 to 200000 elements for L/Deq =1.5 were used. The computational grids used in this work were generated using the set of regions shown in Figure 7.

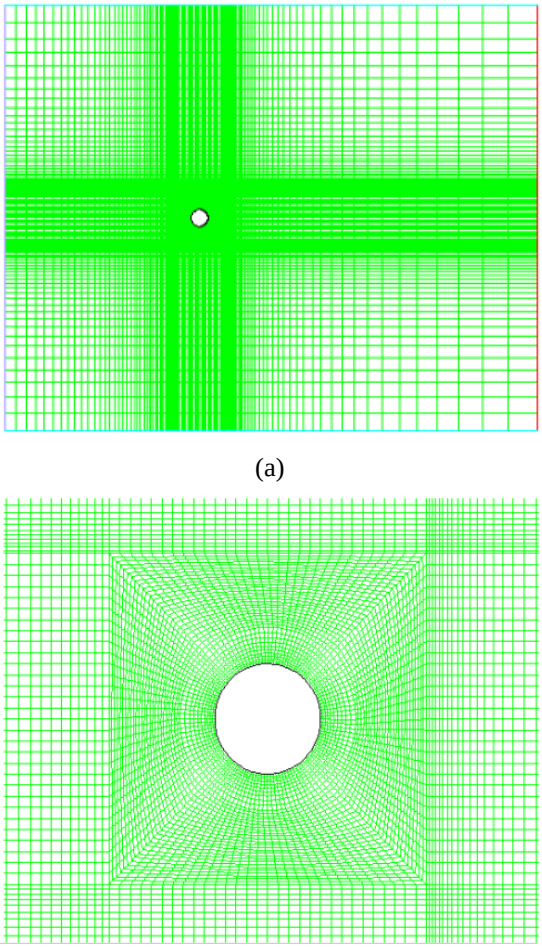

(a)

(b)

Figure 7. Computational Grid: (a) Entire Computational Domain, (b) Closer View around Cylinders

5.1. Vortex Shedding and Strouhal Number

The separation of flow past a circular cylinder causes pairs of eddies to form alternately on the top and bottom part of the cylinder and travel into the wake region resulting in vortex shedding. Vortex shedding is very common in engineering applications. Figures 8-12 show vortex shedding phenomenon in the wake region of the flow past a circular cylinder. Laminar vortex shedding known as the von Karman vortex street has been observed in the wake region of the flow past a circular cylinder at low Reynolds number between 40 to 250. For Reynolds number that is greater than 250, the laminar periodic wake becomes unstable and the eddies start to become turbulent. Further increase of Reynolds number turns the wake region into turbulent flow. Within certain range of Reynolds number ($250 < Re < 10{,}000$), the frequency at which vortices are shed in the flow around a circular cylinder tends to remain almost constant.

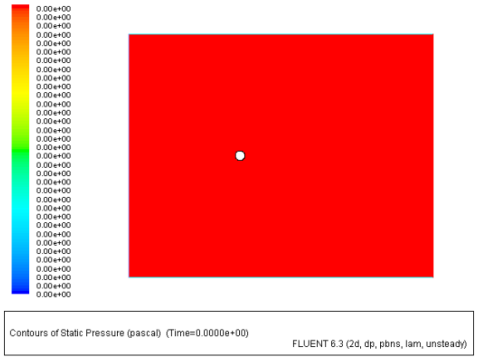

Figure 8. Contours of Static Pressure

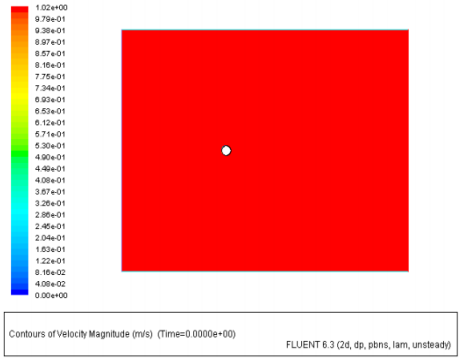

Figure 9. Contours of Velocity Magnitude

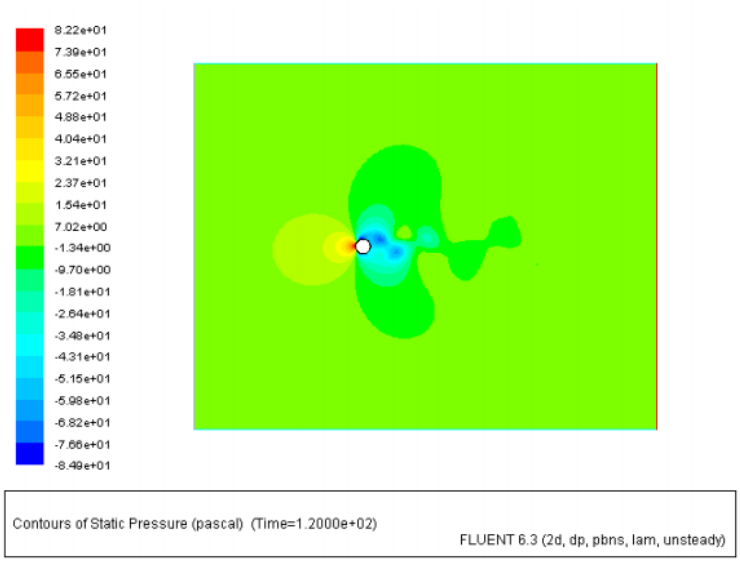

Figure 10. Contours of Static Pressure

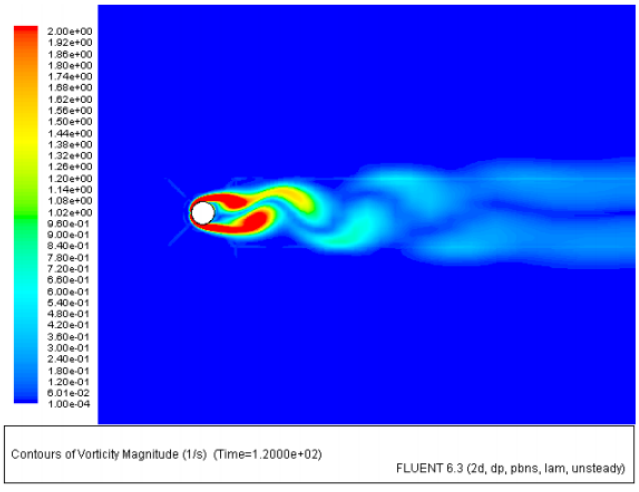

Figure 11. Contours of Vorticity Magnitude

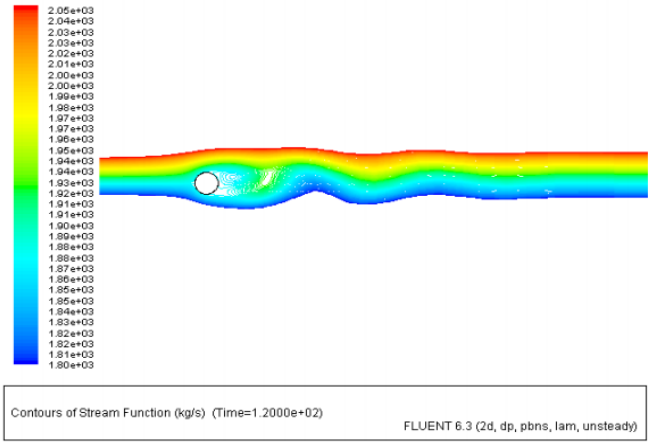

Figure 12. Contours of Stream Function

6. Results

For the purpose of the validation of the solution procedure, it is essential that CFD simulations be compared with experimental data. Fig 13 compares the present results for circular cylinder at subcritical Reynolds numbers (less than 10^7) for drag coefficient with the results of Achenbach [14] and Grove[15]. There is a difference of about 5-9 percent between the present results and the results of experimental studies. It can therefore be concluded that the CFD code can be used to solve the flow fields for similar geometries and conditions.

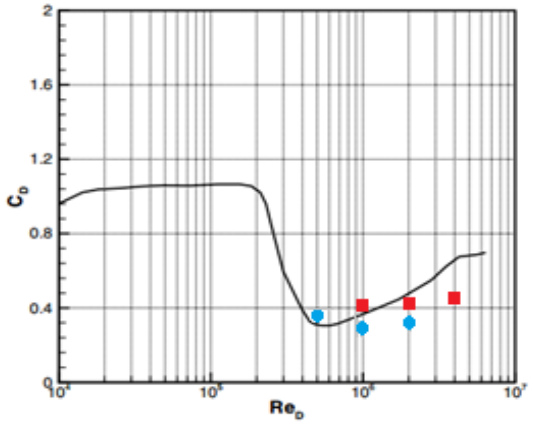

Figure 13. Comparison Drag Coefficient. (—) Achenbach, (•) Grove, (■) Present Work

6.1. Drag and Lift Coefficients

Drag coefficient (C_D) and lift coefficient (C_L) values are monitored during CFD computations and time histories of C_D and C_L are obtained. Periodicity in C_D-history and CL-history graphs shown respectively. Figure 14-15 show time variation of lift and drag Coefficient at $Re=10^5$. indicate the periodic behavior of vortex separation from the surface of the cylinder and its effect on drag and lift forces acting on the cylinder. C_D and C_L are computed by:

$$C_d = 2F_d / (\rho u_\infty^2 A) \quad (7)$$

$$C_L = 2F_L / (\rho u_\infty^2 A) \quad (8)$$

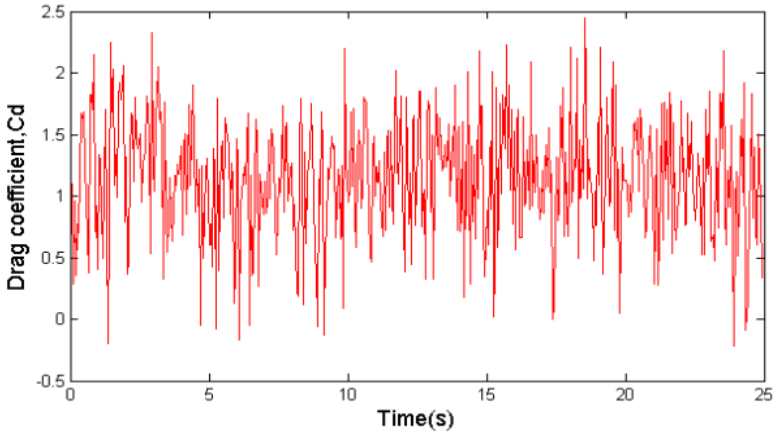

Figure 14. Time Variation of Drag Coefficient at Re=10^5

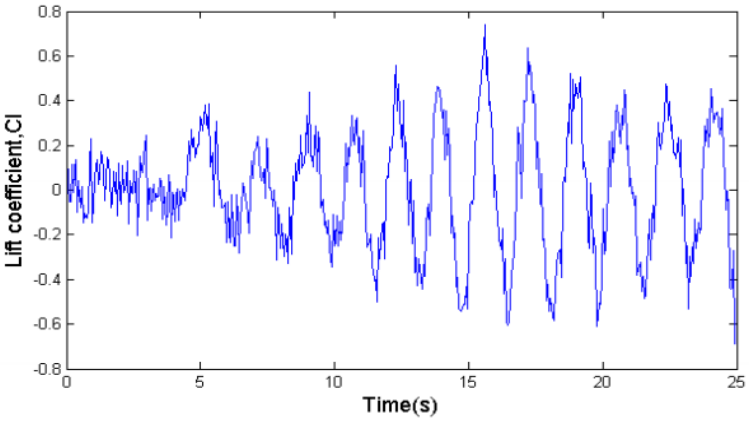

Figure 15. Time Variation of Lift Coefficient at Re=10^5

7. Conclusions

In this study, flow around circular cylinder had been investigated. Investigation covers the effects of high subcritical, supercritical, and transcritical Reynolds numbers and L/D ratio on total drag coefficient. Controlled flow simulations are performed further with the same grid and numerical methods. From this study it is found that the two-dimensional finite volume method computes hydrodynamic forces and captures vortex shedding very well. Even at high Reynolds number, the method is very much applicable without loss of accuracy. Most of the results presented in this research are compared with experimental data and are in better agreement with respect to other numerical results. In this research, 2-D method is found very prospective one for turbulent flow due to its faster convergence. The mean pressure distributions and overall drag coefficients are predicted reasonably well at $Re_D = 0.5\times10^5$ and 1×10^5. The best distances cylinder is L/D_{eq} =1.5. drag coefficient of cylinder for different Reynolds number and various longitudinal pitch ratio being between 2 to 3.

8. List of Symbols

A	Area, m^2
C_D	Drag coefficient, $2F_d/(\rho u_\infty^2 A)$
C_L	Lift coefficient, $2F_L/(\rho u_\infty^2 A)$
D	Large diameter

L	Distance between centers
P	Pressure, circumferential length
Re	Reynolds number [ρUD/μ]
SL	Longitudinal pitch
ST	Transverse pitch
U	x-direction velocity
Δt	Time step
x	x coordinate
y	y coordinate

Greek symbols

ρ	Fluid density
μ	Fluid dynamic viscosity

Subscripts

Cyl	Cylinder
eq	Equivalent

References

[1] R. D. Blevines, "Flow-Induced Vibration", Van Nostrand Reinhold, New York, **(1990)**.
[2] S. Taneda, Journal of Phys. Soc. Japan, vol. 11, no. 302, **(1956)**.
[3] D. J. Tritton, "Experiments on the Flow Past a Circular Cylinder at Low Reynolds Numbers", Journal of Fluid Mech., vol. 6, no. 1, **(1959)**, pp. 547-567.
[4] G. K. Batchelor, "An Introduction to Fluid Mechanics", Cambridge University Press, **(1970)**.
[5] M. M. Zdravkovich, "Flow Around Circular Cylinders" Volume: Fundamentals, Oxford University Press:Oxford, **(1997)**.
[6] A. Thom, "Numerical Solution for the Flow around a Cylinder at Reynolds Numbers of 40, 200 and 500", Proceedings of Roy. Soc. A, vol. 141, no. 1, **(1933)**, pp. 651-669.
[7] A. L. F. Lima-E-Silva, A. Silveira-Neto and J. J. R. Damasceno, "Numerical Simulation of 2- D Flows over a Circular Cylinder, Using the Immersed Boundary Method", Journal of Comp. Physics, vol. 189, no. 2, **(2003)**, pp. 351-370.
[8] J. Park, K. Kwon and H. Choi, "Numerical Solutions of Flow Past a Circular Cylinder at Reynolds Number up to 160", KSME International Journal, vol. 12, no. 1, **(1998)**, pp. 1200.
[9] S. C. R. Dennis and G. Chang, "Numerical Solutions for Steady Flow Past a Circular Cylinder at Reynolds Numbers up to 100", Journal of Fluid Mech., vol. 42, no. 2, **(1970)**, pp. 471-489.
[10] Y. O. Ohya, A. Okajima and M. Hayashi, "Wake Interference and Vortex Shedding", Aerodynamics and Compressible Flow, Gulf Publishing Company: Houston, TX, vol. 8, **(1989)**, pp. 322-389.
[11] C. H. K. Williamson, "Vortex Dynamics in the Cylinder Wake", Annual Review of Fluid Mech., vol. 28, no. 1, **(1996)**, pp. 477-539.
[12] K. Lee and K. S. Yang, "Flow patterns past circular cylinders in proximity", International journal Computers & Fluids, vol. 38, **(2009)**, pp. 778-788.
[13] C. Sweeney and C. Meskell, "Fast Numerical Simulation of Vortex Shedding in Tube Arrays, Using a Discrete Vortex Method", Journal of Fluids and Structures, vol. 18, no. 1, **(2003)**, pp. 501-512.
[14] E. Achenbach, "Distribution of local pressure and skin friction around a circular cylinder in cross-flow up to Re = 5×106", Journal of Fluid Mech., vol. 34, pp. 625-639.
[15] A. S. Grove, F. H. Shair, E. E. Petersen and A. Acrivos, "An Experimental Investigation of the Steady Separated Flow Past a Circular Cylinder", Journal of Fluid Mech., vol. 19, no. 1, **(1964)**, pp. 60-80.

Author

Mojtaba Daneshi was born in 1987. He received his master degree in Department of Mechanical Engineering, Science and Research Branch, I. A. University, Tehran, Iran. His research directions include energy conversion, renewable energy, finite element analysis, experimental and computational fluid dynamics, predictive modeling and optimization of processes.

